Composites: Part A 188 (2025) 108572

Contents lists available at ScienceDirect

Composites Part A

journal homepage: www.elsevier.com/locate/compositesa

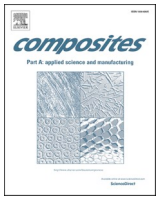

Remaining useful life prediction of flax fibre biocomposites under creep load by acoustic emission and deep learning

Jianqun Hao [a,*], Matthias Rupp [b], Stepan V. Lomov [a], C.A. Fuentes [a,b], Aart W. Van Vuure [a]

[a] Department of Materials Engineering, KU Leuven, Leuven, Belgium
[b] Department of Materials Research and Technology, Luxembourg Institute of Science and Technology, Luxembourg

ARTICLE INFO

Keywords:
A. Natural fibres
B. Creep
D. Acoustic emission
Deep Learning

ABSTRACT

Natural fibre composites are increasingly explored for structural applications due to improvements in mechanical performance. For this, damage prognostics are crucial. We integrate acoustic emission (AE) and deep learning techniques to predict the remaining useful life of a flax fibre composite under long-term creep load. Derivatives of cumulative AE features with respect to time, such as cumulative hit and count rates, are introduced to reflect the performance degradation rate of the materials. These proposed features seem more relevant for creep lifespan than traditional AE features. Long short-term memory networks and temporal convolutional networks are adopted to estimate the composite's remaining useful life. The two models' normalized root mean square errors are below 0.11, less than 20% of the error of a statistical Weibull-distribution benchmark model. Our study demonstrates that AE-based data-driven models can predict the performance degradation of composite materials subject to sustained load.

1. Introduction

Natural fibre composites (NFC) have been increasingly explored for potential structural applications, e.g., in the civil engineering and automotive sectors, owing to notable advancements in optimizing their mechanical performance. Damage prognostics are crucial to ensure the structural integrity and reliability of NFC during their in-service life. When subjected to long-term cyclic (fatigue) and/or constant (creep) loadings, NFC often experience a considerably dispersive lifespan due to the complex deterioration process, which is mainly caused by their non-homogenous characteristics at the composite level, coupled with the non-uniform nature of natural fibres in their micro-structure, component content, as well as the randomly distributed defects like kink bands. In this scenario, the traditional physical or empirical models can only provide a rough lifespan estimation for NFC, because most of the models are formulated in terms of the premeasured ultimate strength and predefined loading patterns [1–6], and overlook the impact of the uncertainty in the damage evolution and accumulation in NFC during their in-service life. Hence, it is necessary to explore a more versatile approach for damage prognostics of NFC under long-term load.

Acoustic emission (AE), a prominent technique in the domain of structural health monitoring, has been widely used in damage detection and identification of composite materials [7–15]. Due to increased requirements in the health management and maintenance of composite structures, efforts have also been made in AE-based damage prognostics to predict the remaining useful life (RUL) and strength (RUS). Compared to simple empirical models considering only a single AE parameter such as energy [16,17] or counts [18] for RUL prediction, AE-based data-driven models have been gaining increased interest due to their excellent capability of processing abundant data and mapping complex non-linear relationships. Several machine-learning methods have been attempted for the damage prognostics of composite materials based on AE data, such as the Gaussian process [19,20], the random forest model [21,22], and artificial neural networks (ANN) [23–30]. However, these methods do not take the temporary dependency in the time-series data into account, which is essential for RUL prediction of composite materials subject to cumulative damage. While Hidden Semi Markov Models (HSMM) [31–33] consider the sequence information and show better performance in RUL prediction of composite materials than an ANN model [34], they are limited to a modestly-sized discrete hidden state space and computationally expensive for modelling long-term dependency [35].

Long Short-Term Memory (LSTM) networks are a variety of recurrent neural networks (RNNs) that are capable of learning long-term

* Corresponding author.
E-mail address: jianqun.hao@kuleuven.be (J. Hao).

https://doi.org/10.1016/j.compositesa.2024.108572
Received 20 August 2024; Received in revised form 16 October 2024; Accepted 31 October 2024
Available online 2 November 2024

dependency. They specialize in discovering the underlying patterns embedded in time series, which makes them suitable to track the degradation process and thus to predict the RUL [36]. Yousef et al. [37] predicted the long-term water absorption and thickness swelling behaviours of wood plastic composites by using an LSTM network and found that 200 h of training data is adequate for the LSTM model to achieve a mean absolute percentage error of 2 % between the actual and predicted data. Nguyen et al. [38] carried out the RUL prediction for a concrete beam under a four-point bending load based on AE data using an LSTM model. Their findings demonstrate a significant performance improvement when benchmarked against simple RNN models.

Another popular type of neural network is the Convolutional Neural Network (CNN) which has been commonly used in Computer Vision. Motivated by its feature extraction ability and computational efficiency, 1D CNN has been introduced to signal processing in the context of structural health monitoring [39,40]. To deal with the problem of temporal dependency existing in RUL prediction, the AE sequential data are often segmented by a time window with fixed or variable length and then fed as an input into the CNN models [41,42]. More recently, a Temporal Convolutional Network (TCN) architecture integrated with dilated causal convolutions and residual blocks, was introduced for sequence learning tasks [43,44] and so far has attracted considerable attention [45–48]. It is claimed the TCN model outperforms mainstream RNN models such as LSTMs and gated recurrent unit neural networks, across a diverse range of sequence modelling tasks and datasets [44].

Despite the tremendous potential of data-driven models such as LSTM and TCN in damage prognostics, very few attempts have been made for RUL prediction in the field of composite materials, especially for natural fibre composites subjected to long-term creep load. In this study, AE sensors and Linear Variable Differential Transformer sensors were employed to detect damage activities and acquire creep deformation information in flax fibre composites during creep rupture tests, respectively. LSTM and TCN models were employed for RUL prediction, and the model performances were compared. Nested cross-validation in conjunction with Bayesian optimization was used to explore the optimal performance level of the two models.

2. Materials and testing

2.1. Material system

The composites were prepared with unidirectional flax fibre (Lineo Flaxtape 110), bound by polyoxymethylene (POM) (Hostaform C2521) through the film stacking method. The UD flax tapes and POM films were predried in an oven at 105 °C for 20 min prior to manufacturing. Two flat stainless-steel plates and one square steel frame were used as the compressing mould. The former was used to compress and heat the materials, while the latter allowed avoiding the lateral flow-away of the molten polymers and controlled the thickness of the composite plates. Eight layers of flax tapes were stacked between nine layers of POM films, achieving a laminate thickness of 1.5 mm with a target fibre volume fraction of 40 %. Two Teflon films were inserted between the surface polymer films and the flat metal plates for demoulding.

The properties of the fibre and matrix as well as their composite are listed in Table 1. The longitudinal strength and modulus of the fibre and matrix were measured by tensile tests, whereas the composites were tested in flexural mode. Tensile and flexural tests were conducted in accordance with the standard test methods ASTM D3039 and ASTM D7264, respectively.

Table 1
Properties of flax fibre and POM as well as their composite.

Materials	Density (g/cm^3)	Longitudinal modulus (GPa)	Longitudinal strength (MPa)
Flax fibre	1.45	68 ± 3.4	533 ± 37
POM	1.41	~2.6	~62
Flax/POM composite	~1.43	19.3 ± 1.7	201 ± 6.5

2.2. Creep rupture tests monitored by AE

The creep rupture tests were performed using a custom-designed flexural creep set-up placed in an environmentally conditioned room (23 °C & 50 % RH) as shown in Fig. 1 (a). Six Linear Variable Differential Transformer sensors (LVDT) with a resolution of 1 μm were attached on the set-up for measuring the deflection of the samples under creep load. Several stainless-steel blocks with varying dimensions were fabricated to apply the constant creep load by connecting the hooks positioned in the middle of the specimens. Through adjusting the number of blocks, a weight resolution of 1 N could be achieved for the sustained load. Four different stress ratios (the ratio of applied stress to the ultimate strength measured by quasi-static flexural tests), namely 90 %, 85 %, 80 % and 75 %, were used to examine the applicability of the proposed strategy. The standard test method ASTM D2990 was consulted to perform the creep tests. The span length of the two support beams is 48 mm in accordance with a span-thickness ratio of 32:1. The creep load was gradually applied over a period of ~ 10 s. More details about this creep set-up can be found in [49].

The AE device (Vallen AMSY-6 system) was used to monitor the creep rupture tests. The acoustic signal was captured by an AE-sensor Digital wave B-1025 with a broadband response from 50 − 2000 kHz, and subsequently amplified by a preamplifier Vallen AEP4 with a 34 dB gain before being processed by AE-signal processor ASIP-2A. A threshold of 30.1 dB was used and the sampling rate of the AE sensors was 10 MHz (100 ns). Tow parameters, discrimination time (400 μ s) and rearm time (1000 μ s), were used to discriminate hits and hit cascades, respectively.

When the samples were loaded in 3-point bending mode during creep tests, the AE activities were concentrated in the middle of the sample where the damage developed, as shown in Fig. 1 (b) where two AE sensors were used for the damage localization. Hence, only one sensor was used for each sample afterwards as the issue of disparity in detected signal energy due to varied source-detector distance (energy attenuation) caused by scattered damage location barely exists. With four data acquisition channels configured in this Vallen system, four creep measurements can be performed synchronously, which significantly reduced the total experimental time.

3. Methodology

The goal of this work is to predict the RUL of flax/POM composites after being subjected to a certain constant load for a period of time, t*. To this end, all the predictors (creep descriptors and AE features) over time collected before t* were fed into the data-driven models for prediction and the RUL before failure is the output of the models. The technical details of data preparation and model architecture are introduced in the following subsections.

3.1. Data preparation

3.1.1. Feature extraction

Different from AE-based damage diagnostics for composite materials where the damage modes are primarily identified by non-cumulative AE features (e.g., amplitude, rise time, counts, energy, frequency), damage prognostics rely more on cumulative features such as cumulative hits, cumulative counts, and cumulative energy, which are sensitive to the damage evolution [17,26,42,50–52]. Furthermore, previous work [53] found that for flax fibre composites the cumulative hits detected during creep rupture tests at various moments in time (“time stamps”) show a similar trend to the damage volume fraction, as determined by micro-computed tomography. This demonstrated that this AE feature is capable of reflecting the damage severity, see Fig. 2 (a).

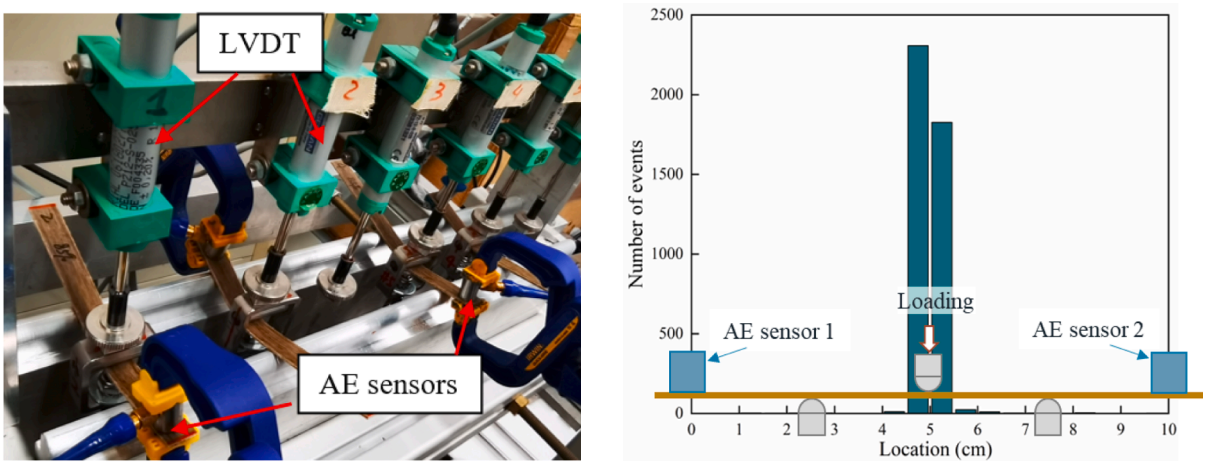

Fig. 1. (a) Creep tests monitored by AE and LVDT. (b) Distribution of AE events along sample lengthwise direction.

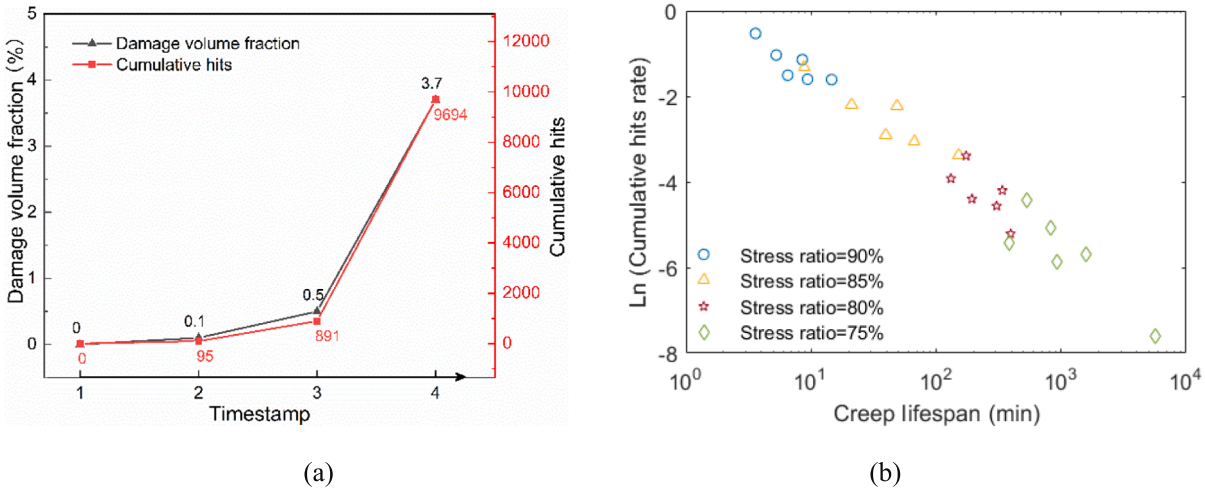

Fig. 2. The cumulative hits detected by AE during long-term creep rupture tests (a) corelation between cumulative hits and damage volume fraction representing the damage severity tracked by micro computed tomography [53]; (b) correlation between the cumulative hits rate of the specimens and the corresponding creep lifespan.

Inspired by this, the cumulative features rate (the first derivative of cumulative features with respect to time) is proposed and regarded as an indicator of degradation rate. As an example, Fig. 2 (b) illustrates the relationship between the creep lifespan and the cumulative hits rate. A significant correlation ($R^2 = 0.96$) can be observed. Hence, twenty-five AE features comprising thirteen non-cumulative features, six cumulative features and six cumulative features rates, were extracted based on AE data, as presented in Table 2.

Creep deformation is a straightforward observation for the structural response when the structure is subjected to long-term creep load. Deformation data can provide valuable information in structural design and the assessment of structural health. For example, creep strain data are often used to calculate safety factors concerning time-dependent creep failure in structural design in civil engineering. The typical creep deformation-related features are creep strain and creep strain rate. The former is associated with material ductility, while the latter can represent the viscosity of the materials. Additionally, creep ratio (the ratio of creep strain at a certain moment to the instantaneous strain) is considered a significant feature of creep lifespan because it can reflect the damage tolerance of the composites when subjected to long-term creep load based on previous study [49]. The typical curves of creep strain, creep rate, and creep ratio of samples during creep rupture tests are illustrated in Fig. 3.

3.1.2. *Feature selection*

Feature selection can reduce the computational cost and improve the model performance by eliminating irrelevant and redundant features. Three filter methods, the ReliefF [54,55], Neighbourhood Component Analysis (NCA) [56], and Minimum Redundancy Maximum Relevance (mRMR)[57] were adopted for feature subset selection considering their computational efficiency and applicability to different machine learning models. The ReliefF algorithm scores the features according to the respective difference values they give to k-nearest neighbours with the same and different response variables. Specifically, the feature weights are penalized if they give different values to the neighbours with the same response, and are rewarded if they give different values to neighbours with different response. NCA is also a nearest neighbour-based feature evaluation method. The main idea of this algorithm is that the feature weights are learned via minimizing a weighted loss function (the average leave-one-out regression error with respect to feature weights), using the gradient descent technique.

While the ReliefF and NCA have been found to be valuable for the

Table 2
Twenty-five extracted AE features.

No.	Feature provided by Vallen system	No.	Extracted feature
1	Amplitude – A (dB)	14	Cumulative hits – Cum_Hits
2	Rise time – RT (μs)	15	Cumulative rise time – Cum_RT (μs)
3	Duration time – DT (μs)	16	Cumulative duration time – Cum_DT (μs)
4	Counts – C	17	Cumulative counts – Cum_C
5	Energy – E (eu)	18	Cumulative energy – Cum_E (eu)
6	Signal strength – SS(nV s)	19	Cumulative signal strength – Cum_SS (nV s)
7	Root mean square – RMS (μV)	20	Cumulative hits rate – Cum_Hits_rate (μs^{-1})
8	Peak frequency– FMAX (kHz)	21	Cumulative rise time rate – Cum_RT_rate
9	Frequency centroid of Gravity– FCOG (kHz)	22	Cumulative duration time rate- Cum_DT_rate
10	Cascade hits – CHIT	23	Cumulative counts rate – Cum_C_rate (μs^{-1})
11	Cascade counts – CC	24	Cumulative energy rate– Cum_E_rate (eu^{-1})
12	Cascade energy – CE (eu)	25	Cumulative signal strength rate – Cum_SS_rate (nV)
13	Cascade signal strength – CSS (nV s)		

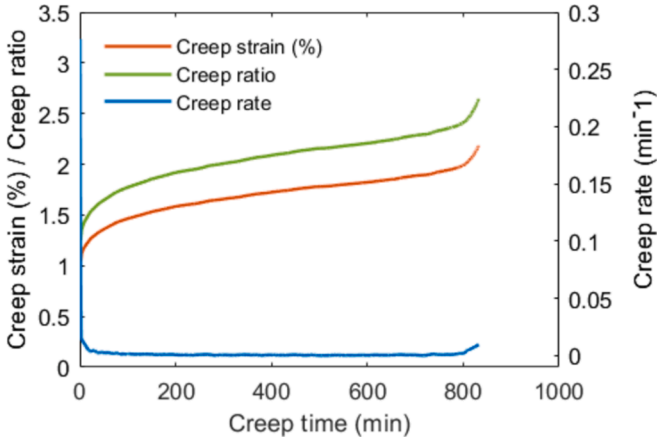

Fig. 3. Typical curves of creep strain, creep rate, and creep ratio during creep rupture tests.

selection of AE features [42], the two methods focus on only the feature relevance/importance to their response variable and are incapable of examining the redundance within the selected features. The mRMR method aims to select the feature subset with the maximal dependency, maximal relevance and the minimal redundancy from the raw feature set. Based on the relevance and redundance measured by mutual information, mRMR can effectively reduce the redundant features while keeping the relevant features for the model. In this study, the ReliefF and NCA were firstly applied to find a candidate feature set, and mRMR was then used to examine the redundancy for selecting a more compact subset.

Fig. 4 (a) and (b) presents the importance of the twenty-eight features (twenty-five AE features and three creep deformation features) with respect to RUL, quantified by ReliefF and NCA. All the non-cumulative AE features, e.g., amplitude, rise time, duration time, etc., show negative importance weights calculated by the ReliefF and approximately zero value by NCA, implying they are not relevant to the RUL. This finding is consistent with the results reported in [42]. Most cumulative AE features and cumulative features rates have positive important weights measured by the ReliefF and relatively large values by NCA, except cumulative energy and cumulative energy rate. The low relevance of cumulative energy and its rate might be due to their poor correlation with the damage evolution of the composite under creep load, as reported in [53]. Cumulative hits rate appears to be the most important health indicator of RUL among the AE features according to ReliefF and NCA, which is in accord with the strong correlation shown in Fig. 2 (b). The three creep deformation features, particularly creep ratio, are significant to the response, as indicated by their relatively high importance values. Hence, the thirteen non-cumulative AE features as well as cumulative energy and cumulative energy rate were eliminated. The remaining AE features, and three creep deformation features were evaluated later by mRMR, as shown in Fig. 4 (b).

Based on the mutual information quotient (relevance/redundancy), these features do not show clear differences in their quotients despite the highest ratio of relevance to redundancy measured for cumulative hits. This indicates they have balanced contribution to RUL and their importance is not significantly different. In other words, there isn't a single dominant feature; instead, multiple features play crucial roles in explaining the variability in the response variable. Therefore, the ten AE features and three creep deformation features presented in Fig. 4 (b) were used as the input of the models.

3.2. Architecture of deep learning models for RUL prediction

3.2.1. Long Short-Term memory (LSTM) model architecture

Several variants of LSTM have been developed in the past years to handle a variety of sequence learning problems since the LSTM cell was first proposed by Hochreiter and Schmidhuber [58]. In this work, a regular unidirectional LSTM comprising input gate, forget gate and output gate, are adopted, as illustrated in Fig. 5 (a). To deal with the RUL prediction task, fully connected layers (FC) are added to map the learned sequential information from the LSTM to the final regression output. Besides, a dropout layer serving as a regularization technique is used to help avoid the overfitting issue. The final LSTM model architecture is presented in Fig. 5 (b).

3.2.2. Temporal convolutional network (TCN) model architecture

The prominent characteristics of a TCN are mainly attributed to its two ingredients, namely causal convolution, and dilation convolution, as depicted in Fig. 6 (a). The former provides a causal constraint that the output at each timestamp is only determined by the historical inputs and not by any "future" inputs, which is a logical design for the prediction of time-series data. The latter is an alternative approach to increasing the filter size and network depth when a long-term dependency needs to be learned from the long historical data. With the dilation operation, the receptive field can be exponentially expanded, which enables an output at the top level to represent a wide range of the inputs.

The residual block [60] is often preferred in TCN models, to speed up convergence and enable training of much deeper models [43,44]. With the dilated causal convolutions and residual connections as the elements, the TCN models can be adjusted for various sequence learning tasks. In this work, the residual block comprises one dilated causal convolution layer, one weight normalization layer to accelerate the training progress, one rectified linear unit (ReLU) as the activation function, and one spatial dropout layer for the regularization. Additionally, a 1x1 convolution is added when the residual input and output have different dimensions. The visualization of the used TCN architecture is shown in Fig. 6 (b).

4. Results and discussion

4.1. RUL prediction based on LSTM and TCN

The Adaptive moment estimation (Adam) optimizer was used for training via gradient descent. All the hyperparameters of the two models were determined through a rough grid search on the data obtained from preliminary tests. In the LSTM model, 300 hidden units were set in the

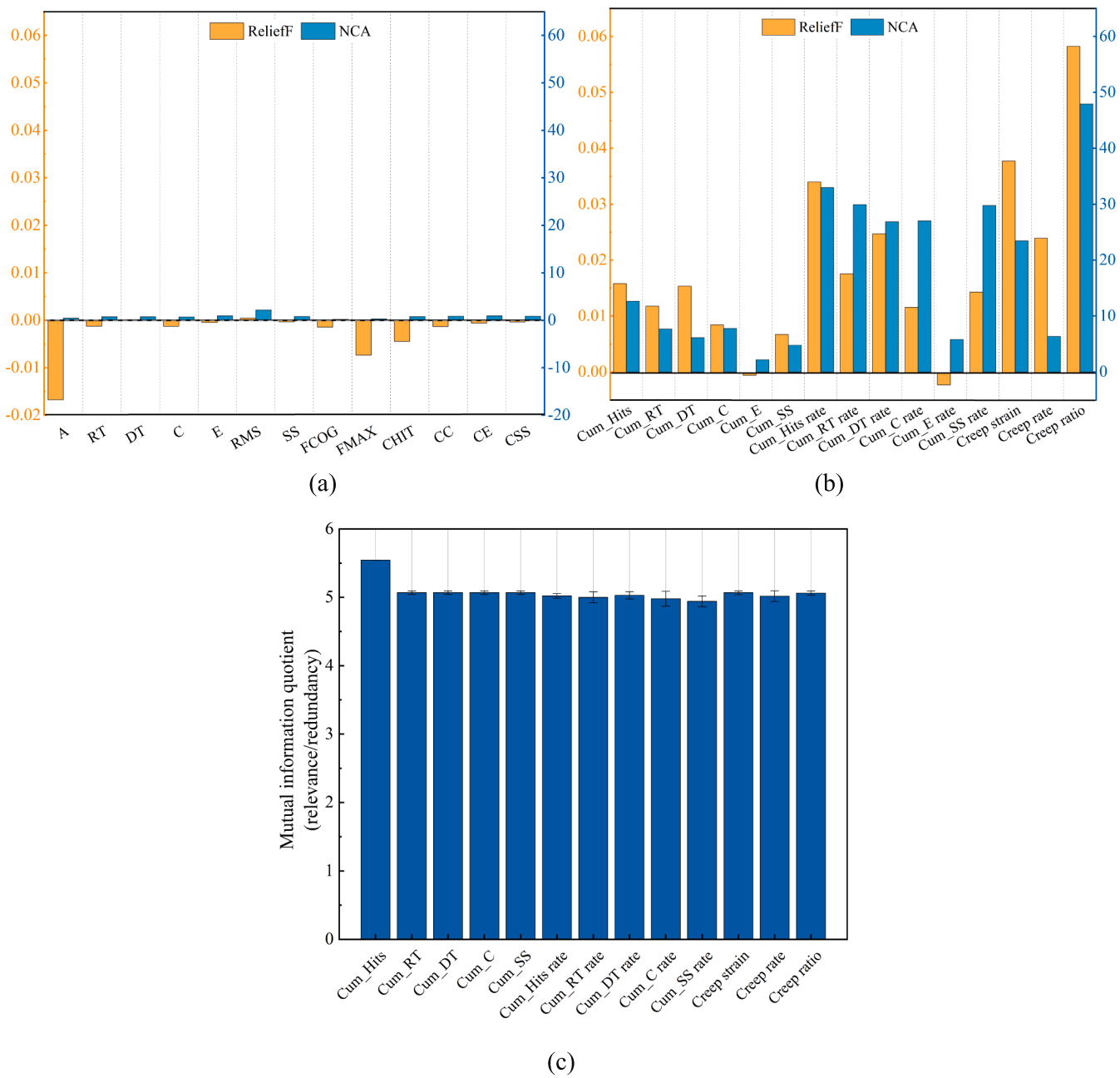

Fig. 4. Importance of (a) non-cumulative AE features (b) cumulative AE features and creep deformation features evaluated by ReliefF and Neighbourhood component analysis (NCA); (c) Redundancy evaluation for a subset of features using Minimum Redundancy Maximum Relevance (mRMR), refer to the list of abbreviations for the features in Table 2.

LSTM layer, followed by a FC layer with 50 neurons. The length of the AE sequential data is ~ 3500 in each measurement. To cover the complete historical data for the predictions at all timestamps, the filter size f of TCN was set as 5 and the number of convolutional layers (residual blocks) $K = 10$ was selected to achieve a receptive field $R = 1 + (f-1)(2^K - 1) = 4093 > 3500$. The number of filters for each convolutional layer was set as 50. The initial learning rate was 0.01 for both LSTM and TCN and reduced by a factor of 0.2 every 50 epochs. The maximum training epoch was set as 200 for LSTM and 100 for TCN as TCN converges more quickly. A dropout rate of 0.5 was used in both models to avoid overfitting.

Given the potentially consistent damage mechanisms and evolution pattern existing in the samples when subjected to different stress levels, an attempt was made to train the models using the data from twenty measurements (five out of six measurements at each stress level), whereas the remaining four measurements were held back for testing. However, poor predictions were obtained when the data from different stress levels were fused, see the results in **Appendix A1**. The reason could be that the features from different stress levels vary widely with respect to time scales, from minutes (under a stress ratio of 90 %) to days (under a stress ratio of 75 %). The diversity of the features at different stress levels might exert a significantly greater influence on the models in training compared to the consistent patterns.

Therefore, the models were trained using data from only the same stress level. A leave-one-out cross-validation method was adopted to estimate the generalization performance of the two models given the relatively small dataset (six measurements for each sample). That is, the data from five measurements of each stress level were used to train the models, and the remaining one measurement was used for testing. Each

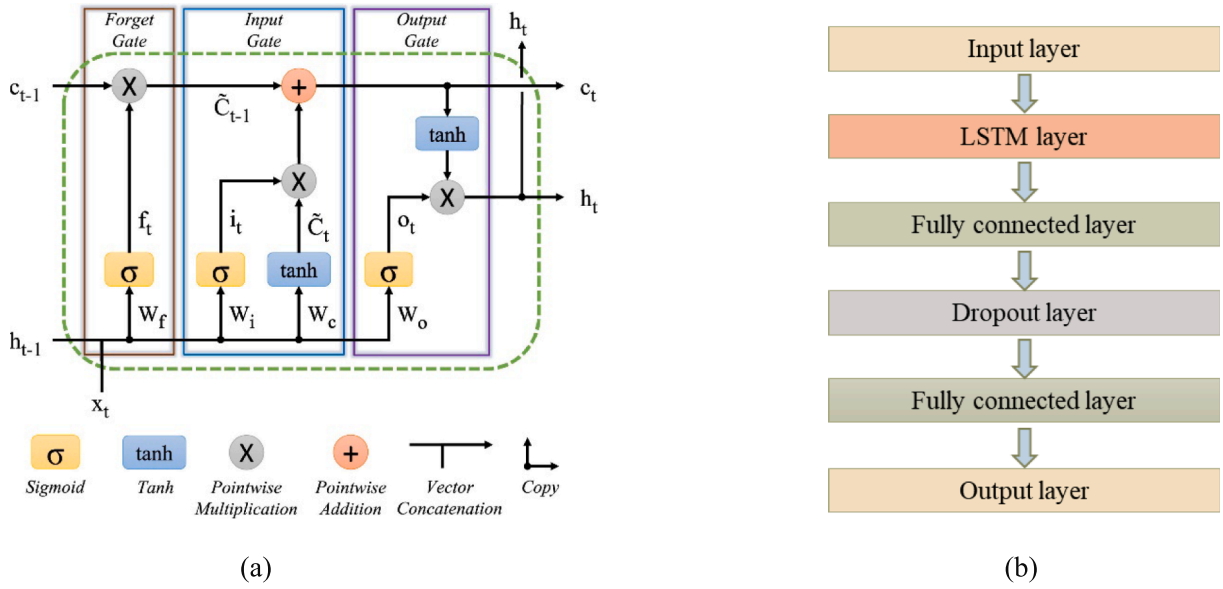

Fig. 5. (a) Diagram of the regular LSTM cell [59]. (b) Architecture of the LSTM model.

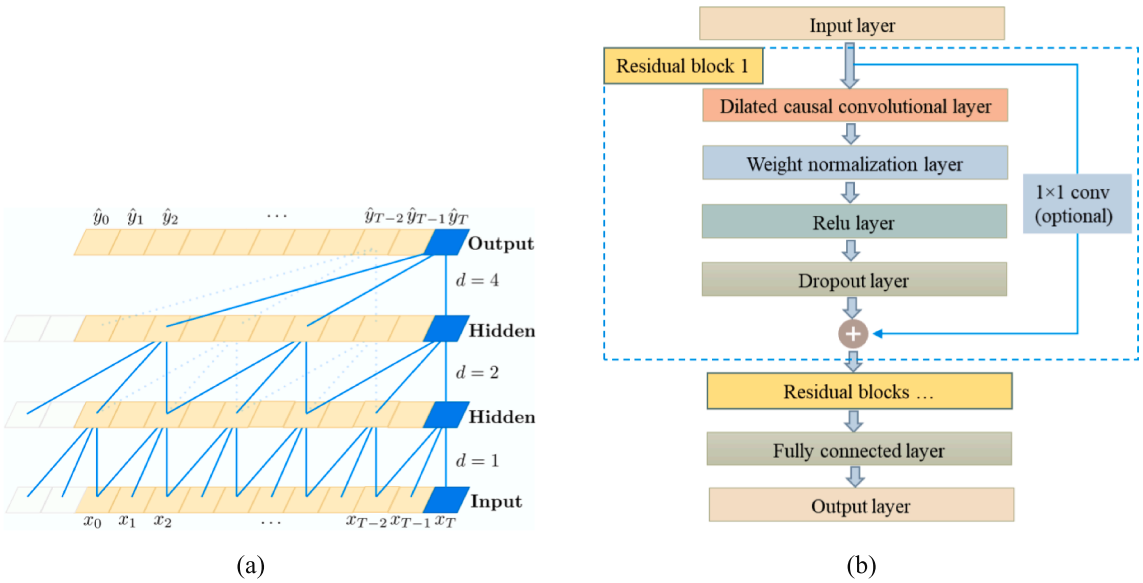

Fig. 6. (a) A dilated causal convolution with dilation factors $d = 1, 2, 4$ and filter size $k = 3$ [44]. (b) Visualization of the TCN architecture.

stress level sample comprises six predictions generated through the leave-one-out cross validation method. While six specimens seem like a small sample size, each specimen generates thousands of AE events, enabling statistical learning. Other related studies have used similar sample sizes, see [21,25,42].

Fig. 7 presents the representative RUL estimations of the four samples (under four different stress ratios) by using LSTM and TCN. The predicted results show satisfactory agreements with the actual RUL overall. It is found that the predicted values deviate noticeably from the actual RUL line in the early stage (most likely the primary creep stage) but converge to the actual RUL line when approaching the end of the creep life. The moderate performance in the early stage is probably because AE events generated sporadically in this stage, leading to a relatively small number of AE events and thus limited information can be fed into the model for prediction.

In order to compare the performance of the two models on the samples under different stress levels, it is essential to select a metric capable of rejecting the influence of significant disparity in their lifespan scale. Mean square error (MSE) and root mean squared error (RMSE) are commonly used criteria for the quantitative assessment of prognostic performance, but they can only provide unbiased evaluation for the data at the same scale. Mean absolute percentage error (MAPE) takes into account the disparity in the life scale by normalizing the absolute errors with corresponding RUL values. For AE data obtained during the damage process of composite materials, however, intensive AE activities are always detected at the last few moments before the end of life. The extremely small actual RUL values tend to give rise to disproportionately large percentage errors, despite the small magnitude of absolute errors. The prediction errors derived from the dense data acquired in the final short period, carry substantial weight when computing the MAPE that represents the overall performance. As a result, an undesirable inflation in MAPE value is often obtained even in the case where good global performance is observed, see examples in [25,34]. In practical applications, the prediction accuracy in the earlier phase draws more attention

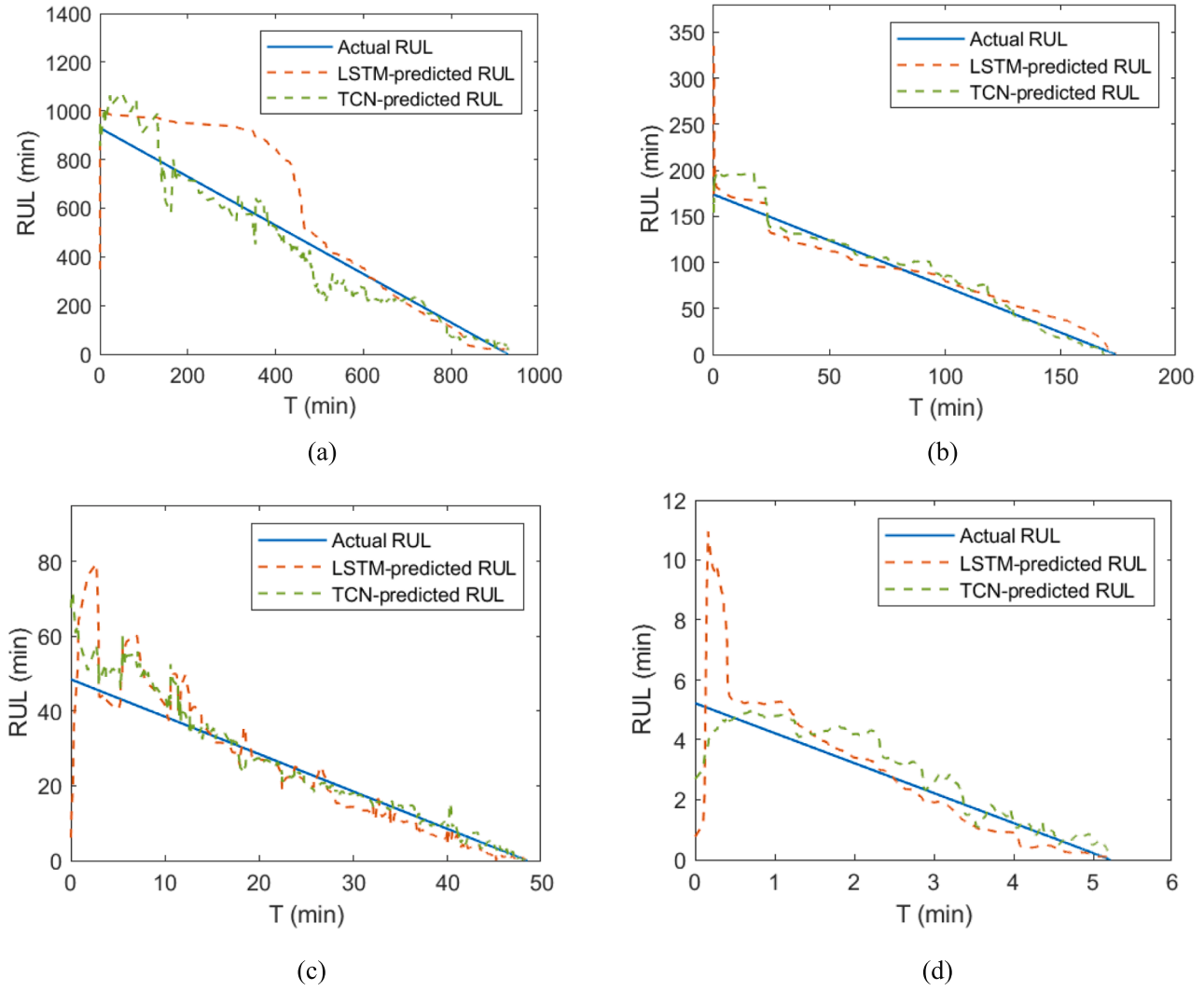

Fig. 7. Representative RUL predictions of samples under four different stress levels: (a) stress ratio of 75%, (b) stress ratio of 80%, (c) stress ratio of 85%, (d) stress ratio of 90%, given by LSTM and TCN. The RUL values at any moment t, were estimated based on the historical data up to t.

since an early warning is more valuable for scheduling maintenance. In this context, it becomes pertinent to assign greater weight (importance) to the predictions made during the early phases, while mitigating the influence of predictions from the latter stages. In this study, RMSE is employed to quantify the prediction errors within each sample. Subsequently, the RMSE values of the samples are normalized by their respective lifespan (NRMSE), to compare the model performance across diverse stress levels. Although the NRMSE underestimates the relative errors notably in the final period, it enables a more coherent assessment of the overall performance and the comparability among different samples. The normalized RMSE is formulated as follows:

$$NRMSE = \frac{RMSE}{T_L} = \frac{\sqrt{\frac{1}{N}\sum_{t=1}^{N}\left(\widehat{RUL}(t) - RUL_{actual}(t)\right)^2}}{T_L} \tag{1}$$

where $\widehat{RUL}_{(t)}$ is the estimated RUL and T_L the corresponding creep lifespan.

To benchmark the performance of the two AE-based data-driven models, the RUL is also analysed statistically using a simple Weibull distribution model:

$$P(t) = 1 - exp\left[-\left(\frac{t}{t_0}\right)^{\beta}\right] \tag{2}$$

where t_0 and β are the scale and shape parameters, respectively.

The lifespan, namely RUL(t = 0) follows well the Weibull distribution, as shown in **Appendix A2**. The estimation of the RUL at any moment is given by a prediction line constructed with a slope of −1, and the mean value of the Weibull distribution model as its intercept.

The corresponding NRMSE values of the two data-driven models and the Weibull distribution model are depicted in Fig. 8 (a). The mean NRMSE illustrated by a black dashed line is used to represent the generalization performance of the three models under four different stress levels. The mean NRMSE values of LSTM and TCN models are close and both are less than 0.11 at the four stress levels, which demonstrates satisfactory predictive capabilities. When benchmarked against the Weibull distribution model, the model errors are merely 20 %, 7 %, 16 %, and 7 % of its performance at stress ratios of 75 %, 80 %, 85 %, and 90 %, respectively.

Among the four stress levels, the sample with a stress ratio of 80 % exhibits the most favourable performance of all the three models. While, higher mean NRMSE values are observed in samples with stress ratios of 75 % and 85 %. One essential reason accounting for the performance disparities among different samples is attributed to the variability of

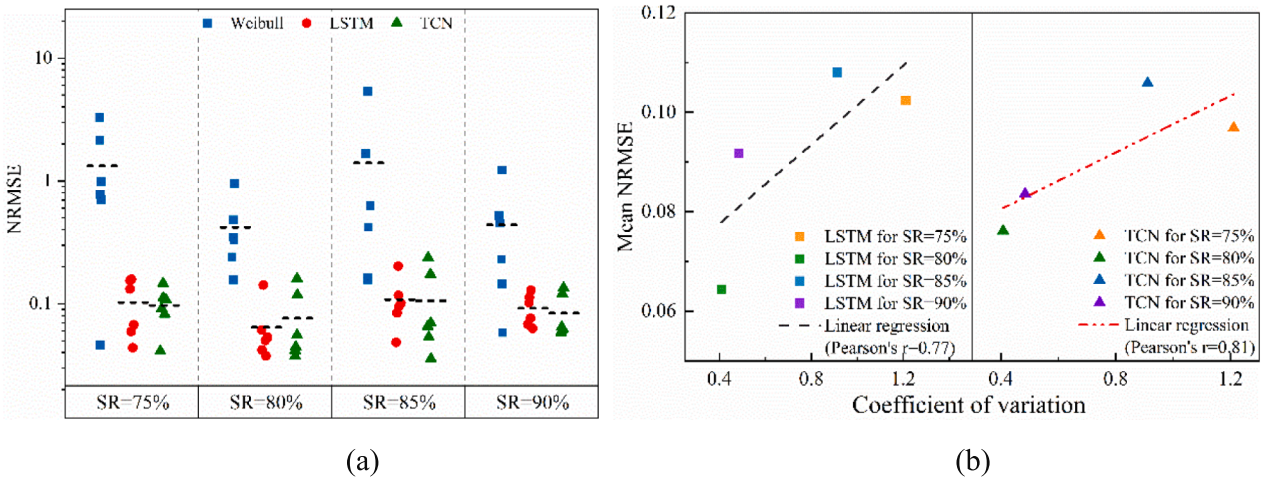

Fig. 8. (a) The normalized RMSE of the two models for the samples under four different stress ratios. (b) The correlation between the coefficient of variation of creep lifespan and the corresponding mean NRMSE.

creep lifespan (the response of the dataset). Here, the coefficient of variation, defined as the ratio of the standard deviation to the mean value, is adopted to quantify the relative variance of the creep lifespan of samples with six measurements under four different stress ratios. Fig. 8 (b) presents the correlation between the coefficients of variation and the NRMSE of the four samples. It is found that the Pearson correlation coefficient between the coefficient of variation and the NRMSE is 0.77 for LSTM and 0.81 for TCN, which demonstrates their model performance is significantly influenced by the variance in the dataset. Higher variance typically implies greater pattern diversity and/or increased noise within the data, posing more significant challenges for the models to discern underlying patterns.

In comparison with LSTM, TCN demonstrates lower mean NRMSE values across most samples, which indicates its better performance in handling the task in this study. Additionally, TCN offers a computational efficiency advantage due to its parameter sharing mechanism, which utilizes same filters, significantly reducing the number of parameters required. This reduction can lead to a faster training process, see **Appendix A3**. However, a greater sensitivity to data variance is evident, as indicated by the Pearson correlation coefficient. Overall, TCN might be a more promising method for the prediction of time-series data.

4.2. *Nested cross-validation and Bayesian optimization*

In pursuit of optimizing the performance of both models within the constraints of limited data due to the time cost of long-term creep tests, a more sophisticated hyperparameter tuning strategy compared to simple grid or random search, namely Bayesian optimization, was adopted to refine the hyperparameters of the two models. It leverages information from previous evaluations to intelligently select the next set of hyperparameters for exploration and exploitation, which enables the algorithm to focus its efforts on regions where the probability of attaining the most promising performance scores is highest. In Bayesian optimization, the mapping between the hyperparameter combinations and the objective function (validation error) that has no closed-form expression is drawn from a probabilistic model, a Gaussian process. To determine the next point for evaluation, the expected improvement acquisition function was used in this study. More details about Bayesian optimization can be found in [61].

A nested cross-validation approach is adopted to avoid optimistically

Fig. 9. Illustration of nested leave-one-out cross-validation.

biased estimation of performance resulting from using the same dataset for hyperparameter tuning and performance evaluation. Fig. 9 depicts the framework of nested leave-one-out cross-validation (CV) in conjunction with Bayesian optimization. The outer loop is responsible for error estimation, while the inner loop CV serves for hyperparameter tuning. For each outer loop, the dataset is split into six folds (six measurements in each sample) in which five folds are used for training and the remaining one for testing. In the inner loop, one fold of the training data from the outer loop is held back as the validation set and the remaining four folds are used for model training. The hyperparameter combinations are first explored through Bayesian optimization. The optimal model configuration is determined by assessing the cross-validated metric (mean error) on the five validation datasets. Afterwards, the generalization performance of the two models is evaluated with the mean error of the optimal models for the six outer loops.

The sample with a stress ratio of 80 % was selected as an example to present the performance improvement of the two models with Bayesian optimization. RMSE is used as the metric to compare the model performance on the same sample. The hyperparameters to be tuned in the LSTM model include the number of LSTM units in the hidden layer with a search domain from 10 to 500, the number of units in the FC layer ranging from 10 to 100, and the initial learning rate from 0.0001 to 1. Fig. 10 (a) provides a representative plot which shows the RMSE of the LSTM model varying with 100 different combinations of the three hyperparameters. The RMSE values are indicated with the size of the solid circle and the accompanying colour bar attached on the right of the graph. It is seen that the data points are nonuniformly distributed across the entire search space. Instead, they are densely clustered in a specific region where the lowest RMSE is eventually found. The lower RMSE could be theoretically achieved before exhaustively exploring all possible hyperparameter combinations. To confirm the best observation found within 100 iterations with a high confidence level when dealing with an infinite number of potential combinations, the lowest RMSE values observed so far over each iteration are presented in Fig. 10 (b).

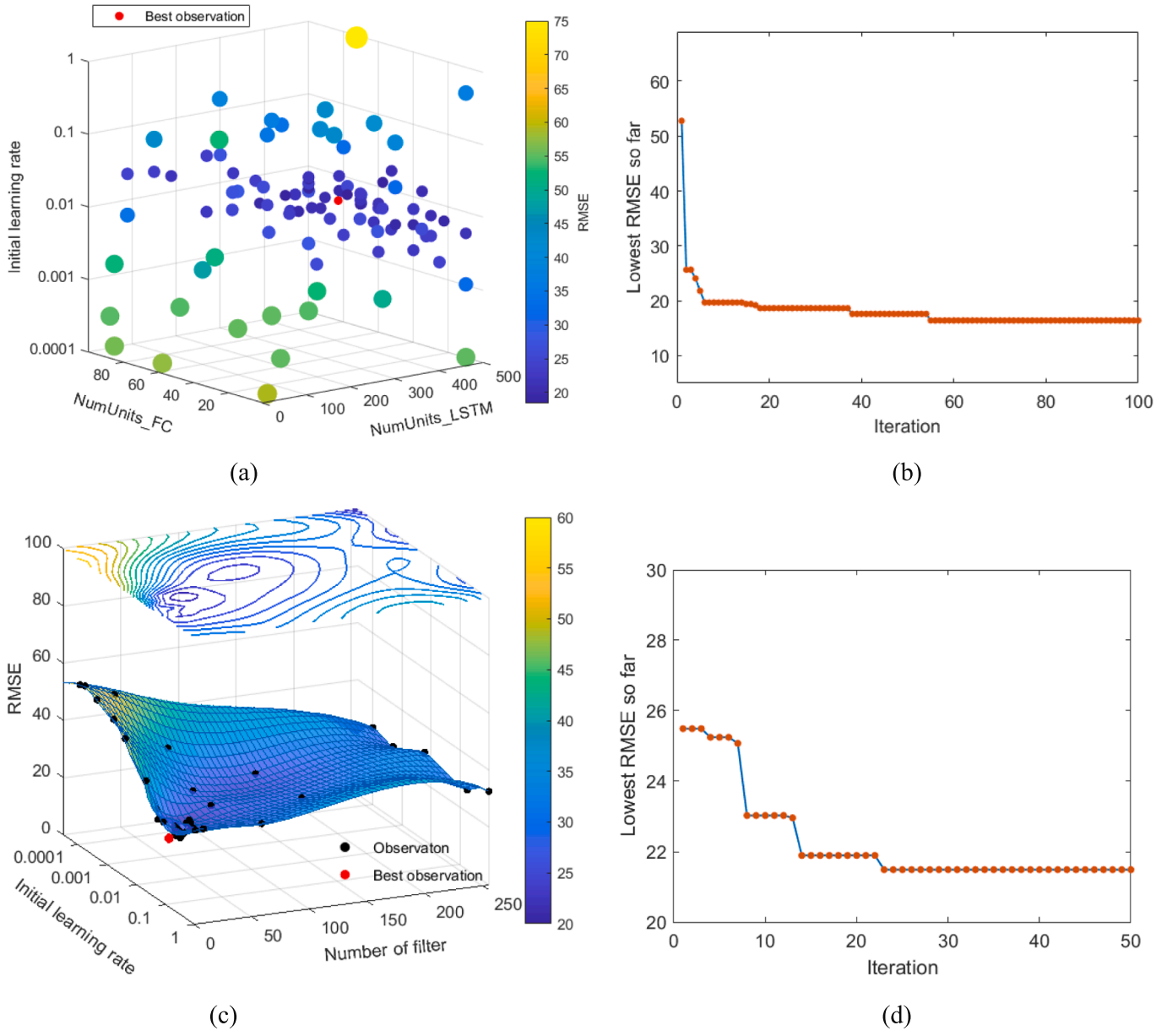

Fig. 10. Hyperparameter tuning for the LSTM and TCN models: (a) RMSE varying with number of units in fully connected layer, number of LSTM units and initial learning rate of the LSRM model; (b) the lowest RMSE value of the LSTM model over the iterations (different hyperparameter combinations); (c) RMSE varying with number of filters and initial learning rate of the TCN model; (d) the lowest RMSE value of the TCN model over the iterations.

The lowest RMSE is updated if the current hyperparameter combinations lead to a lower RMSE than the lowest value in previous iterations. It is found that lower RMSE of the LSTM model is continuously observed until 55 iterations and the remaining 45 iterations fail to yield a lower RMSE value. This suggests that the hyperparameter combination leading to the lowest RMSE is most probably the optimal setting, even with only 100 iterations.

In the TCN model, the number of residual blocks and the filter size are justified to cover the complete historical data. The other hyperparameters which appear to be significant are the number of filters ranging from 2 to 512 with an exponential variation based on 2, and initial learning rate from 0.0001 to 1. Fig. 10 (c) presents the observed RMSE values (linked to z axis) of the TCN model with respect to the two hyperparameters within 50 iterations. A 3 D surface is used to fit the discrete RMSE observations, and a contour is superposed on the top of the graph. The RMSE values of the surface and the contour are linked with a colour bar on the right. The surface plot shows an approximate distribution of the RMSE in terms of the initial learning rate and the number of filters. Simultaneously, the contour lines provide a clear indication of the locations of local minima, including the global minimum corresponding to the lowest RMSE, denoted by a red solid circle. The lowest RMSE value is identified at the 23rd iteration, as shown in Fig. 10 (d).

The optimal hyperparameter combinations of LSTM and TCN models determined in the inner loop CV using Bayesian optimization are shown in Table 3. The surrogate model performance is then evaluated on the testing folds in the outer loops and compared with that using rough grid search. The performance improvement percentage (PIP) is given by:

$$PIP = 100 \times \frac{(RMSE_{Bayes-opt} - RMSE_{Grid})}{RMSE_{Grid}} \quad (3)$$

The initial learning rate in the LSTM model shows close values across all testing folds, except for one anomaly observed in testing fold 4, which might be induced by the data noise. In the TCN model, the values of the initial learning rate obtained on all six testing folds are noticeably larger compared to 0.01 determined by grid search, demonstrating the necessity of the refining procedure. The number of LSTM units, the number of neurons in the FC layer of the LSTM model, and the number of filters in the TCN model exhibit a relatively high variance on six testing folds. One possible explanation is that the three hyperparameters appear to have less impact on model performance compared to the initial learning rate, which can be perceived in Fig. 10 (a) and (c). Clearly, the model performance demonstrates an overall improvement when Bayesian optimization is applied, even though a minor performance degradation of 5.9 % is observed in testing fold 2 of the LSTM model. On average, a PIP of 14.2 % and 12.1 % is achieved for the LSTM and TCN models, respectively.

5. Conclusions and outlook

In this study, the RUL of flax fibre composite subjected to creep load was predicted using LSTM and TCN deep learning models based on AE data and creep deformation. Cumulative feature rates, which appear to be significant to the RUL, were proposed to reflect the performance degradation rate of the composites under creep load and incorporated as part of the input variables of the models. A specific metric, NRMSE, was used to assess and compare the model performance across four diverse samples with lifespan spanning three orders of magnitude. The LSTM and TCN models are very close in NRMSE; both outperform the Weibull distribution model. A pronounced correlation (the Pearson correlation coefficient of 0.77 is observed for LSTM, and 0.81 for TCN) between the model performance and the variance of RUL in each sample was observed. In comparison with the LSTM model, TCN exhibits better predictions across the majority of samples, but with a heightened sensitivity to data variance.

Bayesian optimization was used to fine-tune the hyperparameters of the two models using nested CV. An overall improvement of 14.2 % and 12.1 % was obtained for LSTM and TCN models compared to hyperparameter optimization with a rough grid search, respectively.

Although this study demonstrates the applicability of the AE-based data-driven model for RUL prediction of composite materials subjected to long-term creep load, the robustness of the models needs to be further explored for the following reasons. Firstly, the models are scored based on limited data derived from samples subjected to specific loading conditions. This limited dataset may not fully capture the complexities of various loading scenarios. Secondly, the model performance is highly related to the quality of extracted features. The interpretability and relevance of these features may vary across different material compositions, structural configurations, and loading conditions, etc. Additionally, the AE waves are not necessarily consistent even in the same scenario, since they are also affected by factors such as sensor type, sensor-source distance (attenuation issue), and signal acquisition-related user-defined parameters. Therefore, it is imperative to reconstruct and retrain the models, and use them cautiously when dealing with other similar RUL prediction tasks based on AE data.

Several considerations are given for future work:

- The creep tests were conducted under high stress levels (90 %, 85 %, 80 % and 75 %). It would be valuable to generalize the models for lower stress levels. However, evaluating the model performance at low stress levels is a challenge as creep lifespans can extend over centuries, making data difficult to obtain. One potential approach to obtain the data at low stress levels is to accelerate the creep behaviour of the composites using the time–temperature superposition principle. Investigating this approach in future research could provide important insights.
- The AE features are often correlated to the damage mechanisms in the composite materials, and different damage mechanisms have varying impacts on the remaining useful life. Therefore, incorporating the damage classification into the lifespan prediction models could potentially further enhance their accuracy and performance.

Table 3
The optimal hyperparameter combinations of LSTM and TCN models determined by using Bayesian optimization and the performance improvement percentage (PIP) compared to the rough grid search.

Optimization approach	Testing fold	LSTM				TCN		
		Number of LSTM units	Number of neurons in FC layer	Initial learning rate	PIP	Number of filters	Initial learning rate	PIP
Rough grid search	Fold 1–6	300	50	0.01	0.0 %	32	0.01	0.0 %
Bayesian optimization	Fold 1	280	90	0.01558	16.7 %	16	0.06575	8.9 %
	Fold 2	350	100	0.01136	−5.9 %	64	0.04555	17.5 %
	Fold 3	210	100	0.01440	16.1 %	64	0.08755	0.7 %
	Fold 4	310	90	0.00574	6.6 %	128	0.05318	7.1 %
	Fold 5	290	30	0.01799	35.1 %	32	0.03404	26.4 %
	Fold 6	470	60	0.01689	16.4 %	64	0.01978	12.2 %
	Average	–	–	–	14.2 %	–	–	12.1 %

- Techniques such as transfer learning and data augmentation could be explored to deal with the challenge of insufficient creep lifespan data, see the typical work in [62,63]. To enhance the model generalization across varying materials, loading conditions and test environments, physics-informed machine learning models represent a promising solution to address the issues posed by limited representative datasets from different scenarios. By embedding appropriate physics knowledge (laws, principles, or constraints) into the learning process, the models become not only more interpretable but also more effective at generalizing to new scenarios [64].

CRediT authorship contribution statement

Jianqun Hao: Writing – original draft, Validation, Methodology, Investigation, Formal analysis, Data curation, Conceptualization. **Matthias Rupp:** Writing – review & editing, Validation, Methodology, Formal analysis. **Stepan V. Lomov:** Writing – review & editing, Validation, Methodology, Formal analysis. **Carlos Fuentes Rojas:** Writing – review & editing, Supervision. **Aart Willem Van Vuure:** Writing – review & editing, Validation, Supervision, Project administration, Funding acquisition.

Declaration of competing interest

The authors declare that they have no known competing financial interests or personal relationships that could have appeared to influence the work reported in this paper.

Acknowledgments

The authors gratefully acknowledge the financial support from the China Scholarship Council (202006830003, China) and the Interreg NWE Smart Circular Bridge project (No. NWE 993, EU).

Appendix A. Supplementary data

Supplementary data to this article can be found online at https://doi.org/10.1016/j.compositesa.2024.108572.

Data availability

Data will be made available on request.

References

[1] Epaarachchi JA, Clausen PD. An empirical model for fatigue behavior prediction of glass fibre-reinforced plastic composites for various stress ratios and test frequencies. Compos A Appl Sci Manuf 2003;34:313–26. https://doi.org/10.1016/S1359-835X(03)00052-6.
[2] D'Amore A, Grassia L. Comparative study of phenomenological residual strength models for composite materials subjected to fatigue: predictions at constant amplitude (CA) loading. Materials (Basel) 2019:12. https://doi.org/10.3390/ma12203398.
[3] D'Amore A, Grassia L. A method to predict the fatigue life and the residual strength of composite materials subjected to variable amplitude (VA) loadings. Compos Struct 2019;228. https://doi.org/10.1016/j.compstruct.2019.111338.
[4] Guedes RM. Lifetime predictions of polymer matrix composites under constant or monotonic load. Compos A Appl Sci Manuf 2006;37:703–15. https://doi.org/10.1016/j.compositesa.2005.07.007.
[5] Guedes RM. Creep and fatigue lifetime prediction of polymer matrix composites based on simple cumulative damage laws. Compos A Appl Sci Manuf 2008;39:1716–25. https://doi.org/10.1016/j.compositesa.2008.07.014.
[6] Samareh-Mousavi SS, Taheri-Behrooz F. A new phenomenological creep residual strength model for the life prediction of the laminated composites. Fatigue Fract Eng Mater Struct 2021;44:3152–68. https://doi.org/10.1111/ffe.13574.
[7] Kersani M, Lomov SV, Van Vuure AW, Bouabdallah A, Verpoest I. Damage in flax/epoxy quasi-unidirectional woven laminates under quasi-static tension. J Compos Mater 2015;49:403–13. https://doi.org/10.1177/0021998313519282.
[8] Barile C, Casavola C, Pappalettera G, Vimalathithan PK. Damage characterization in composite materials using acoustic emission signal-based and parameter-based data. Compos B Eng 2019;178. https://doi.org/10.1016/j.compositesb.2019.107469.
[9] Sikdar S, Liu D, Kundu A. Acoustic emission data based deep learning approach for classification and detection of damage-sources in a composite panel. Compos B Eng 2022;228. https://doi.org/10.1016/j.compositesb.2021.109450.
[10] Aslan M. Investigation of damage mechanism of flax fibre LPET commingled composites by acoustic emission. Compos B Eng 2013;54:289–97. https://doi.org/10.1016/j.compositesb.2013.05.042.
[11] Carvelli V, D'Ettorre A, Lomov SV. Acoustic emission and damage mode correlation in textile reinforced PPS composites. Compos Struct 2017;163:399–409. https://doi.org/10.1016/j.compstruct.2016.12.012.
[12] Pei N, Zhou S, Xu C, Shang J, Wu Q. Cluster analysis of acoustic emission signals for tensile damage characterization of quasi-static indented carbon/glass fiber-reinforced hybrid laminate composites. Compos A Appl Sci Manuf 2021:150. https://doi.org/10.1016/j.compositesa.2021.106597.
[13] Oz FE, Ersoy N, Mehdikhani M, Lomov SV. Multi-instrument in-situ damage monitoring in quasi-isotropic CFRP laminates under tension. Compos Struct 2018;196:163–80. https://doi.org/10.1016/j.compstruct.2018.05.006.
[14] Fan Su Y, Yu Zhang T, Sun H, Hua Ma L, Zhou W. Cryogenic damage behavior of carbon fiber reinforced polymer composite laminates via fiber-optic acoustic emission. Compos A Appl Sci Manuf 2024;186:108435. https://doi.org/10.1016/j.compositesa.2024.108435.
[15] Liu Y, Huang K, xin Wang Z, Li Z, Chen L, Shi Q, et al. Cross-scale data-based damage identification of CFRP laminates using acoustic emission and deep learning. Eng Fract Mech 2023;294:109724. https://doi.org/10.1016/j.engfracmech.2023.109724.
[16] Momon S, Moevus M, Godin N, R'Mili M, Reynaud P, Fantozzi G, et al. Acoustic emission and lifetime prediction during static fatigue tests on ceramic-matrix-composite at high temperature under air. Compos A Appl Sci Manuf 2010;41:913–8. https://doi.org/10.1016/j.compositesa.2010.03.008.
[17] Racle E, Godin N, Reynaud P, Fantozzi G. Fatigue lifetime of ceramic matrix composites at intermediate temperature by acoustic emission. Materials (Basel) 2017;10. https://doi.org/10.3390/ma10060658.
[18] Philippidis TP, Assimakopoulou TT. Using acoustic emission to assess shear strength degradation in FRP composites due to constant and variable amplitude fatigue loading. Compos Sci Technol 2008;68:840–7. https://doi.org/10.1016/j.compscitech.2007.08.012.
[19] Liu Y, Mohanty S, Chattopadhyay A. A Gaussian process based prognostics framework for composite structures. Model Signal Process Control Smart Struct 2009;2009(7286):72860J. https://doi.org/10.1117/12.815889.
[20] Liu Y, Mohanty S, Chattopadhyay A. Condition based structural health monitoring and prognosis of composite structures under uniaxial and biaxial loading. J Nondestr Eval 2010;29:181–8. https://doi.org/10.1007/s10921-010-0076-2.
[21] Louis SYM, Nasiri A, Bao J, Cui Y, Zhao Y, Jin J, et al. Remaining useful strength (RUS) prediction of SiCf-SiCm composite materials using deep learning and acoustic emission. Appl Sci 2020;10. https://doi.org/10.3390/APP10082680.
[22] Nasiri A, Bao J, Mccleeary D, Louis SYM, Huang X, Hu J. Online damage monitoring of SiCf-SiCm composite materials using acoustic emission and deep learning. IEEE Access 2019;7:140534–41. https://doi.org/10.1109/ACCESS.2019.2943210.
[23] Leone C, Caprino G, de Iorio I. Interpreting acoustic emission signals by artificial neural networks to predict the residual strength of pre-fatigued GFRP laminates. Compos Sci Technol 2006;66:233–9. https://doi.org/10.1016/j.compscitech.2005.04.032.
[24] Ramasamy P, Sampathkumar S. Prediction of impact damage tolerance of drop impacted WGFRP composite by artificial neural network using acoustic emission parameters. Compos B Eng 2014;60:457–62. https://doi.org/10.1016/j.compositesb.2013.12.028.
[25] Galanopoulos G, Milanoski D, Eleftheroglou N, Broer A, Zarouchas D, Loutas T. Acoustic emission-based remaining useful life prognosis of aeronautical structures subjected to compressive fatigue loading. Eng Struct 2023;290. https://doi.org/10.1016/j.engstruct.2023.116391.
[26] Suresh Kumar C, Arumugam V, Sengottuvelusamy R, Srinivasan S, Dhakal HN. Failure strength prediction of glass/epoxy composite laminates from acoustic emission parameters using artificial neural network. Appl Acoust 2017;115:32–41. https://doi.org/10.1016/j.apacoust.2016.08.013.
[27] Arumugam V, Shankar RN, Sridhar BTNN, Stanley AJ. Ultimate strength prediction of carbon/epoxy tensile specimens from acoustic emission data. J Mater Sci Technol 2010;26:725–9. https://doi.org/10.1016/S1005-0302(10)60114-4.
[28] Rajendraboopathy S, Sasikumar T, Usha KM, Vasudev ES. Artificial neural network a tool for predicting failure strength of composite tensile coupons using acoustic emission technique. Int J Adv Manuf Technol 2009;44:399–404. https://doi.org/10.1007/s00170-008-1874-x.
[29] Rohman MN, Hidayat MIP, Purniawan A. Prediction of composite fatigue life under variable amplitude loading using artificial neural network trained by genetic algorithm. AIP Conf Proc 2018;1945. Doi: 10.1063/1.5030241.
[30] Liu Y, Huang K, Ding J, Yu S, Li Z, Zhang L, et al. Acoustic emission-based failure load prediction for plain woven laminates under quasi-static indentation. Compos Sci Technol 2024;245. https://doi.org/10.1016/j.compscitech.2023.110355.
[31] Eleftheroglou N, Zarouchas D, Benedictus R. An adaptive probabilistic data-driven methodology for prognosis of the fatigue life of composite structures. Compos Struct 2020;245. https://doi.org/10.1016/j.compstruct.2020.112386.
[32] Eleftheroglou N, Zarouchas D, Loutas T, Alderliesten R, Benedictus R. Structural health monitoring data fusion for in-situ life prognosis of composite structures. Reliab Eng Syst Saf 2018;178:40–54. https://doi.org/10.1016/j.ress.2018.04.031.
[33] Eleftheroglou N, Loutas T. Fatigue damage diagnostics and prognostics of composites utilizing structural health monitoring data and stochastic processes. Struct Heal Monit 2016;15:473–88. https://doi.org/10.1177/1475921716646579.

[34] Loutas T, Eleftheroglou N, Zarouchas D. A data-driven probabilistic framework towards the in-situ prognostics of fatigue life of composites based on acoustic emission data. Compos Struct 2017;161:522–9. https://doi.org/10.1016/j.compstruct.2016.10.109.
[35] Zheng S, Ristovski K, Farahat A, Gupta C. Long Short-Term Memory Network for Remaining Useful Life estimation. 2017 IEEE Int Conf Progn Heal Manag ICPHM 2017 2017:88–95. Doi: 10.1109/ICPHM.2017.7998311.
[36] Zhang J, Wang P, Yan R, Gao RX. Long short-term memory for machine remaining life prediction. J Manuf Syst 2018;48:78–86. https://doi.org/10.1016/j.jmsy.2018.05.011.
[37] Yousefi E, Shiri MB, Rezaei MA, Rezaei S, Band SS, Mosavi A, et al. A novel long-term water absorption and thickness swelling deep learning forecast method for corn husk fiber-polypropylene composite. Case Stud Constr Mater 2022;17. https://doi.org/10.1016/j.cscm.2022.e01268.
[38] Nguyen TK, Ahmad Z, Kim JM. A scheme with acoustic emission hit removal for the remaining useful life prediction of concrete structures. Sensors 2021;21. https://doi.org/10.3390/s21227761.
[39] Kiranyaz S, Ince T, Abdeljaber O, Avci O, Gabbouj M. 1-D Convolutional Neural Networks for Signal Processing Applications. ICASSP, IEEE Int Conf Acoust Speech Signal Process - Proc 2019;2019-May:8360–4. Doi: 10.1109/ICASSP.2019.8682194.
[40] Kiranyaz S, Avci O, Abdeljaber O, Ince T, Gabbouj M, Inman DJ. 1D convolutional neural networks and applications: a survey. Mech Syst Sig Process 2021;151. https://doi.org/10.1016/j.ymssp.2020.107398.
[41] Yang H, Zhao F, Jiang G, Sun Z, Mei X. A novel deep learning approach for machinery prognostics based on time windows. Appl Sci 2019;9. https://doi.org/10.3390/app9224813.
[42] Xu D, Liu PF, Chen ZP. A deep learning method for damage prognostics of fiber-reinforced composite laminates using acoustic emission. Eng Fract Mech 2022;259. https://doi.org/10.1016/j.engfracmech.2021.108139.
[43] Van den Oord A, Dieleman S, Zen H, Simonyan K, Vinyals O, Graves A, et al. WaveNet: A Generative Model for Raw Audio 2016:1–15.
[44] Bai S, Kolter JZ, Koltun V. 2018 An Empirical Evaluation of Generic Convolutional and Recurrent Networks for Sequence Modeling.
[45] Wan R, Mei S, Wang J, Liu M, Yang F. Multivariate temporal convolutional network: a deep neural networks approach for multivariate time series forecasting. Electron 2019. https://doi.org/10.3390/electronics8080876.
[46] Lu X, Ling Y, Liu S. Temporal convolutional network with wavelet transform for fall detection. J Sensors 2022. https://doi.org/10.1155/2022/7267099.
[47] Gan Z, Li C, Zhou J, Tang G. Temporal convolutional networks interval prediction model for wind speed forecasting. Electr Pow Syst Res 2021;191. https://doi.org/10.1016/j.epsr.2020.106865.
[48] Pandey A, Wang D. 2019 TCNN : TEMPORAL CONVOLUTIONAL NEURAL NETWORK FOR REAL-TIME SPEECH ENHANCEMENT IN THE TIME DOMAIN Department of Computer Science and Engineering , The Ohio State University , USA Center for Cognitive and Brain Sciences , The Ohio State University , USA: 6875–9.
[49] Hao J, Bardon J, Mertz G, Fuentes CA, Van Vuure AW. Effect of plasma treatment on hygrothermal creep behaviour of flax fibre composite. Compos A Appl Sci Manuf 2024:185. https://doi.org/10.1016/j.compositesa.2024.108322.
[50] Lissek F, Haeger A, Knoblauch V, Hloch S, Pude F, Kaufeld M. Acoustic emission for interlaminar toughness testing of CFRP: evaluation of the crack growth due to burst analysis. Compos B Eng 2018;136:55–62. https://doi.org/10.1016/j.compositesb.2017.10.012.
[51] Caprino G, Teti R, De Iorio I. Predicting residual strength of pre-fatigued glass fibre-reinforced plastic laminates through acoustic emission monitoring. Compos B Eng 2005;36:365–71. https://doi.org/10.1016/j.compositesb.2005.02.001.
[52] Barile C, Casavola C, Pappalettera G, Paramsamy Kannan V, Kannan VP, Paramsamy Kannan V. Damage monitoring of carbon fibre reinforced polymer composites using acoustic emission technique and deep learning. Compos Struct 2022;292. https://doi.org/10.1016/j.compstruct.2022.115629.
[53] Hao J, Prapavesis A, Lomov SV, Fuentes CA, Willem A, Vuure V, et al. Damage evolution in flax fibre composite under creep load. Compos Struct 2024;329. https://doi.org/10.1016/j.compstruct.2023.117786.
[54] Robnik-Šikonja M, Kononenko I. Theoretical and empirical analysis of ReliefF and RReliefF. Mach Learn 2003;53:23–69.
[55] Robnik-Šikonja M, Kononenko I. An adaptation of Relief for attribute estimation in regression. Mach {L}earning {P}roceedings {F}ourteenth Int Conf 1997;5:296–304.
[56] Yang W, Wang K, Zuo W. Neighborhood component feature selection for high-dimensional data. J Comput 2012;7:162–8. https://doi.org/10.4304/jcp.7.1.161-168.
[57] Hanchuan Peng, Fuhui Long and CD. 2005 Feature Selection Based on Mutual Information :Criteria of Max-Dependency, Max-Relevance, and Min-Redundancy; 27:1226–38.
[58] Hochreiter S, Schmidhuber J. Long short-term memory. Neural Comput 1997;9:1735–80. https://doi.org/10.1162/neco.1997.9.8.1735.
[59] Shah SR Bin, Chadha GS, Schwung A, Ding SX. 2021 A Sequence-to-Sequence Approach for Remaining Useful Lifetime Estimation Using Attention-augmented Bidirectional LSTM. Intell Syst with Appl;10–11. Doi: 10.1016/j.iswa.2021.200049.
[60] He K, Zhang X, Ren S, Sun J. 2016 Deep residual learning for image recognition. Proc IEEE Comput Soc Conf Comput Vis Pattern Recognit; -Decem:770–8. Doi: 10.1109/CVPR.2016.90.
[61] Frazier PI. A Tutorial on Bayesian Optimization 2018:1–22.
[62] Du J, Zeng J, Wang H, Ding H, Wang H, Bi Y. Using acoustic emission technique for structural health monitoring of laminate composite: a novel CNN-LSTM framework. Eng Fract Mech 2024;309. https://doi.org/10.1016/j.engfracmech.2024.110447.
[63] Zhao J, Xie W, Yu D, Yang Q, Meng S, Lyu Q. Deep transfer learning approach for localization of damage area in composite laminates using acoustic emission signal. Polymers (Basel) 2023;15:1–14. https://doi.org/10.3390/polym15061520.
[64] Maia MA, Rocha IBCM, Kovačević D, van der Meer FP. Physically recurrent neural network for rate and path-dependent heterogeneous materials in a finite strain framework. Mech Mater 2024;198:1–28. https://doi.org/10.1016/j.mechmat.2024.105145.